Structural, dielectric, and ferroelectric properties of lead-free BCZT ceramics elaborated by low-temperature hydrothermal processing

Zouhair Hanani, Daoud Mezzane, M'barek Amjoud, Yaovi Gagou, Khalid Hoummada, Carine Perrin, Anna Razumnaya, Zdravko Kutnjak, Adnane Bouzina, Mimoun El Marssi, et al.

Structural, dielectric, and ferroelectric properties of lead-free BCZT ceramics elaborated by low-temperature hydrothermal processing

Zouhair Hanani[1,2] · Daoud Mezzane[1] · M'barek Amjoud[1] · Yaovi Gagou[3] · Khalid Hoummada[4] · Carine Perrin[4] · Anna G. Razumnaya[3,5] · Zdravko Kutnjak[6] · Adnane Bouzina[1] · Mimoun El Marssi[3] · Mohamed Gouné[2] · Brigita Rožič[6]

Abstract

Lead-free $Ba_{0.85}Ca_{0.15}Zr_{0.10}Ti_{0.90}O_3$ (BCZT) ceramics have demonstrated excellent dielectric, ferroelectric, and piezoelectric properties in comparison to lead-based materials. The synthesis of pure and crystalline BCZT nanopowders at low temperatures of 25, 80, and 160 °C was reported previously by using a sol–gel method followed by a hydrothermal route. In this study, the structural, dielectric, and ferroelectric properties of sintered BCZT ceramics at 1250 °C/10 h were investigated. XRD measurements revealed the presence of a single perovskite phase at room temperature with the coexistence of the orthorhombic and tetragonal symmetries. The increase of grain size and the ceramic density in BCZT ceramics result in an enhancement of the dielectric and ferroelectric properties of BCZT ceramics. More interestingly, the synthesis temperature of BCZT powders with high dielectric and ferroelectric properties could be decreased to a low temperature of 160 °C, which is about 1200 °C lower when compared with solid-state reaction and 840 °C lower when compared with sol–gel methods. The BCZT ceramics elaborated at 160 °C revealed excellent electrical properties (dielectric constant, dielectric loss, remnant polarization, and maximal polarization of 12,085, 0.017, 8.59 μC/cm^2, and 27.21 μC/cm^2, respectively) and enhanced energy performances (recovered energy density and energy efficiency of 367.2 mJ/cm^3 and 67.2%, respectively). Hence, the use of low-temperature hydrothermal processing can be encouraging for the synthesis of lead-free ceramics with high dielectric and ferroelectric properties.

1 Introduction

Lead-based materials like $PbZr_xTi_{1-x}O_3$ (PZT) have been thoroughly investigated in last decades due to their outstanding dielectric, ferroelectric, and piezoelectric properties for application in energy storage devices, capacitors, transducers, and sensors [1, 2]. However, their possible toxicity limits their applications in future. Correspondingly, new lead-free materials were developed recently to mimic properties of lead-based materials [3–5].

In 2009, Liu and Ren [6] reported $Ba_{0.85}Ca_{0.15}Zr_{0.10}Ti_{0.90}O_3$ (BCZT) ceramic with excellent dielectric and electromechanical properties at the morphotropic phase boundary (MPB) comparable to lead-based materials. However, a large and growing body of literature is based on high-temperature synthesis to make pure and crystalline BCZT powder [7–9]. The first published synthesis of BCZT complex composition was based on solid-state reaction at high temperatures (calcination at 1350 °C and sintering between 1450–1500 °C) due to its simplicity and capability to obtain enhanced dielectric, ferroelectric, and piezoelectric performances [6]. Subsequently, BCZT ceramic was elaborated by soft chemistry routes like sol–gel [7], citrate reaction [10], solvothermal [11], and hydrothermal [12]. However, relative high temperature is needed to obtain pure and crystalline BCZT powder. Jaimeewong et al. [13] outlined a comparative study of two BCZT ceramics synthesized by solid-state and sol–gel auto-combustion methods at 1200 °C and 900 °C, respectively. Quite recently, we reported the effect of grain size

✉ Zouhair Hanani
zouhair.hanani@edu.uca.ma

1 IMED-Lab, Cadi Ayyad University, 40000 Marrakesh, Morocco

2 ICMCB, University of Bordeaux, 33600 Pessac, France

3 LPMC, University of Picardy Jules Verne, 80039 Amiens, France

4 IM2NP, Aix Marseille University, 13397 Marseille, France

5 Faculty of Physics, Southern Federal University, Rostov-on-Don 344090, Russia

6 Jožef Stefan Institute, 1000 Ljubljana, Slovenia

on the dielectric properties of BCZT ceramic via surfactant-assisted solvothermal processing at low-temperature sintering [11]. Enhanced dielectric and ferroelectric properties were obtained using the anionic surfactant SDS (sodium dodecyl sulfate). However, the high calcination temperature (1000 °C) limits the application of BCZT ceramic in the energy-efficient industrial fields.

Since, the energy consumption reduction is one of the crucial aspects for industrial application of ferroelectric ceramics, and to overcome the drawback of calcination, we raised a challenge to elaborate pure and crystalline BCZT ceramic at very-low temperature without calcination step. Previously, we reported the synthesis of scalable BCZT ceramics at low temperature including room temperature (25 °C) [14]. The key strategy is to elaborate BCZT ceramics using two-step synthesis to overcome the low reactivity of Zr ions [15, 16]. First, sol–gel to obtain $Zr_{0.10}Ti_{0.90}O_2$, then addition of barium and calcium salts to obtain pure BCZT crystalline nanopowders by hydrothermal route. More recently, Ji et al. [17] reported the effects of synthesis time on the structure, morphology, and size distribution of the powders of BCZT ceramic elaborated by sol–gel hydrothermal reaction at 180 °C. However, high sintering temperature (1400 °C) was required to obtain enhanced dielectric, ferroelectric, and piezoelectric properties. In this study, we aim to evaluate the structural, morphological, dielectric, and ferroelectric properties of BCZT ceramics sintered at low sintering temperature (1250 °C) using powders elaborated at very-low temperature (25, 80, and 160 °C) [14].

2 Experimental

2.1 BCZT Powders synthesis

BCZT pure and scalable nanocrystalline powders were obtained through sol–gel method followed by a single-step hydrothermal synthesis in high alkaline medium as reported previously [14]. Briefly, B-25, B-80, and B-160 powders were elaborated using sol–gel to elaborate $Zr_{0.1}Ti_{0.9}O_2$ (ZTO) nanopowder, then hydrothermal reaction of ZTO with barium acetate and calcium nitrate at 25, 80, and 160 °C for 24 h, respectively. For electrical measurements, BCZT powders were uni-axially pressed into pellets of diameter about 6 mm and thickness about 1 mm, and then sintered at 1250 °C/10 h.

2.2 Characterization

Crystalline structure of BCZT ceramics was determined by X-ray diffraction (XRD, Rigaku) using a Cu-K_α radiation ($\lambda \sim 1.540593$ Å). The resulting microstructures were analyzed by using a Scanning Electron Microscope (SEM, Tescan VEGA3). The grain size distributions of BCZT ceramics were determined by using ImageJ software. The density of the sintered ceramics was measured by Archimedes method using deionized water as a medium. A precision LCR Meter (HP 4284A, 20 Hz to 1 MHz) was used to measure the dielectric properties of gold-sputtered BCZT pellets in the frequency range of 20 Hz to 1 MHz. The ferroelectric hysteresis loops were determined by using a ferroelectric test system (AiXACCT, TF Analyzer 3000).

3 Results and discussion

3.1 Morphological study

Figure 1 displays the SEM micrographs and the variation of bulk and relative densities and grain size with synthesis temperature for BCZT ceramics sintered at 1250 °C/10 h. B-25 exhibits small grain with an average of 0.8 µm (Fig. 1a) and small density of 4.70 g/cm^3. Increasing the hydrothermal reaction temperature to 80 °C results in BCZT ceramics with small and coarse spheroidal grains with a small increase in the grain size average (2.5 µm) and enhanced bulk density of 5.2 g/cm^3 (Fig. 1b). A further increase in the temperature to 160 °C (B-160), BCZT ceramic with coarse and flatten grains (grain size of 22.1 µm) and well-defined grain boundary was observed. This leads to an improvement of the bulk density to 5.62 g/cm^3, which corresponds to 97.1% of the theoretical density (5.789 g/cm^3).

3.2 Structural study

Figure 2 reveals the XRD patterns of BCZT ceramics elaborated at different temperatures. As we reported previously in the as-prepared BCZT powders [14], all the sintered BCZT ceramics have a pure perovskite phase, without any secondary phase peaks, which indicates that the stabilization of the ferroelectric phases was already reached in BCZT powders. The diffraction peaks of all samples shift to higher 2θ values by increasing the hydrothermal temperature (Fig. 2b). In other words, diffraction peaks shift to higher diffraction angles as grain size increases as seen in SEM images in Fig. 1. These suggest a decreasing of BCZT unit cell, and/or the reduction of defects and the structural relaxation [18, 19]. Meanwhile, the splitting of peaks observed around 45° (Fig. 2c) and the formation of triplets at 65.8° (Fig. 2d) demonstrate the coexistence of orthorhombic (*Amm2*) and tetragonal phases (*P4mm*) at the morphotropic phase boundary (MPB) in BCZT ceramics [11, 14, 20–22].

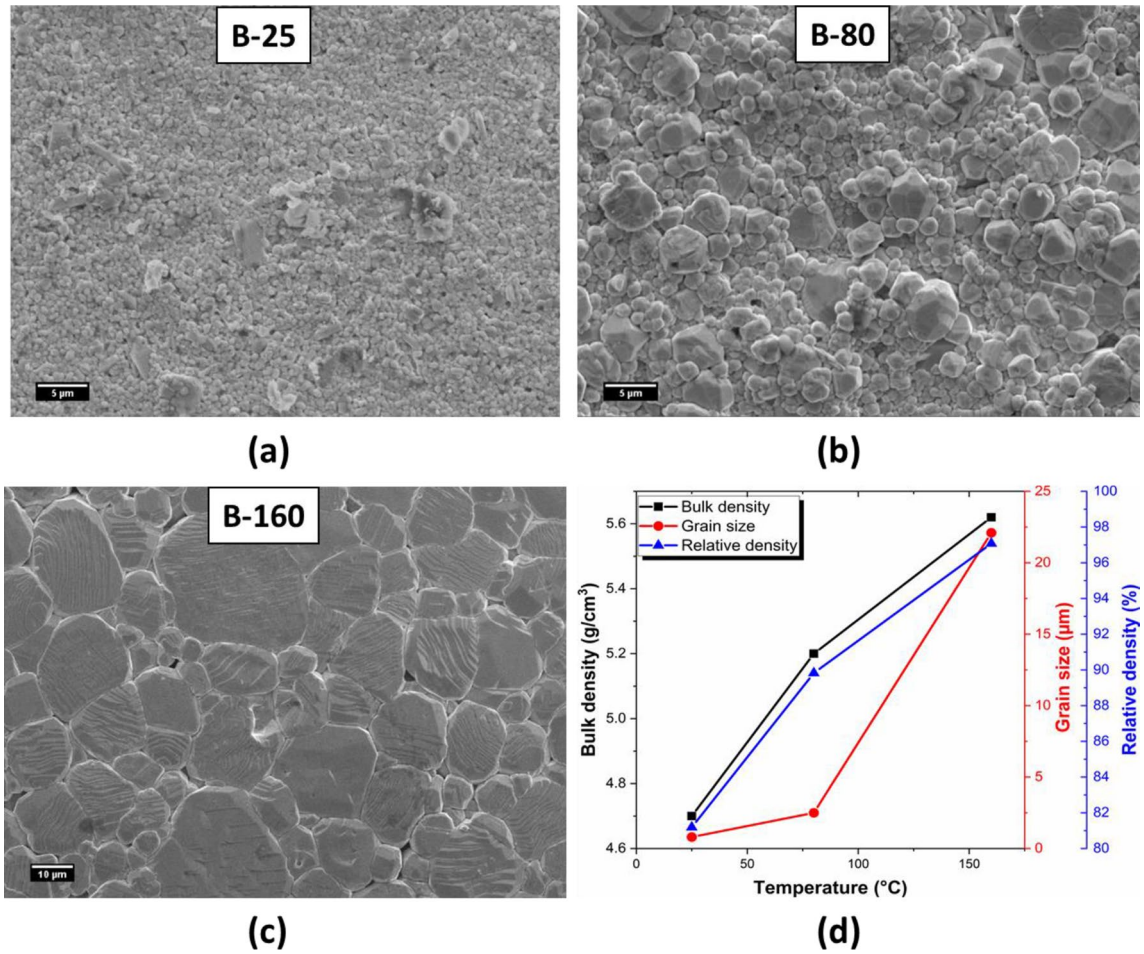

Fig. 1 SEM micrographs of **a** B-25, **b** B-80, and **c** B-160 ceramics sintered at 1250 °C/10 h and **d** variation of bulk and relative densities and grain size with synthesis temperature

3.3 Dielectric properties

Figure 3a compares the temperature dependence of the dielectric constant and dielectric loss at 1 kHz of B-25, B-80, and B-160 ceramics sintered at 1250 °C/10 h. All samples exhibit a broad dielectric anomaly associated with tetragonal-cubic (*T*–*C*) phase transition (Fig. 3a). Meanwhile, the dielectric losses of all samples decrease gradually when increasing measurement temperature to 40 °C, then remain constant, and after that they increase (Inset of Fig. 3a). The overall dielectric properties at 1 kHz of all ceramics are summarized in Table 1. The temperature dependence of the dielectric constant and the dielectric loss of all BCZT ceramics at various frequencies are shown in Fig. 3b–d. The dielectric properties were enhanced with increasing hydrothermal temperature. Despite the low sintering temperature of B-160 ceramic, the maximal value of the dielectric constant reached a value of 12,085, which is much higher than that reported in other works using solvothermal [11], hydrothermal [12], or sol–gel hydrothermal routes [17]. Moreover, for all BCZT samples, the peak temperatures are frequency dependent and shifted to higher temperature with increasing frequency (reminiscent of relaxor behavior) [23, 24].

Curie–Weiss law (Eq. 1) could help to properly understand this phase transition. For this purpose, the inverse dielectric constant as a function of temperature at 1 kHz was plotted and fitted. Figure 4a, c, e and Table 1 display the plots and fitting results.

$$\frac{1}{\varepsilon_r} = \frac{T - T_0}{C}\left(T > T_0\right), \tag{1}$$

where ε_r is the real part of the dielectric constant, T_0 is the Curie Weiss temperature, and C is the Curie–Weiss constant.

It is worth noting that ε_r of all samples deviate from the Curie–Weiss law above the T_c. Equation (2) evaluates this deviation by introducing ΔT_m that is defined as [8],

$$\Delta T_m(K) = T_{dev} - T_m, \tag{2}$$

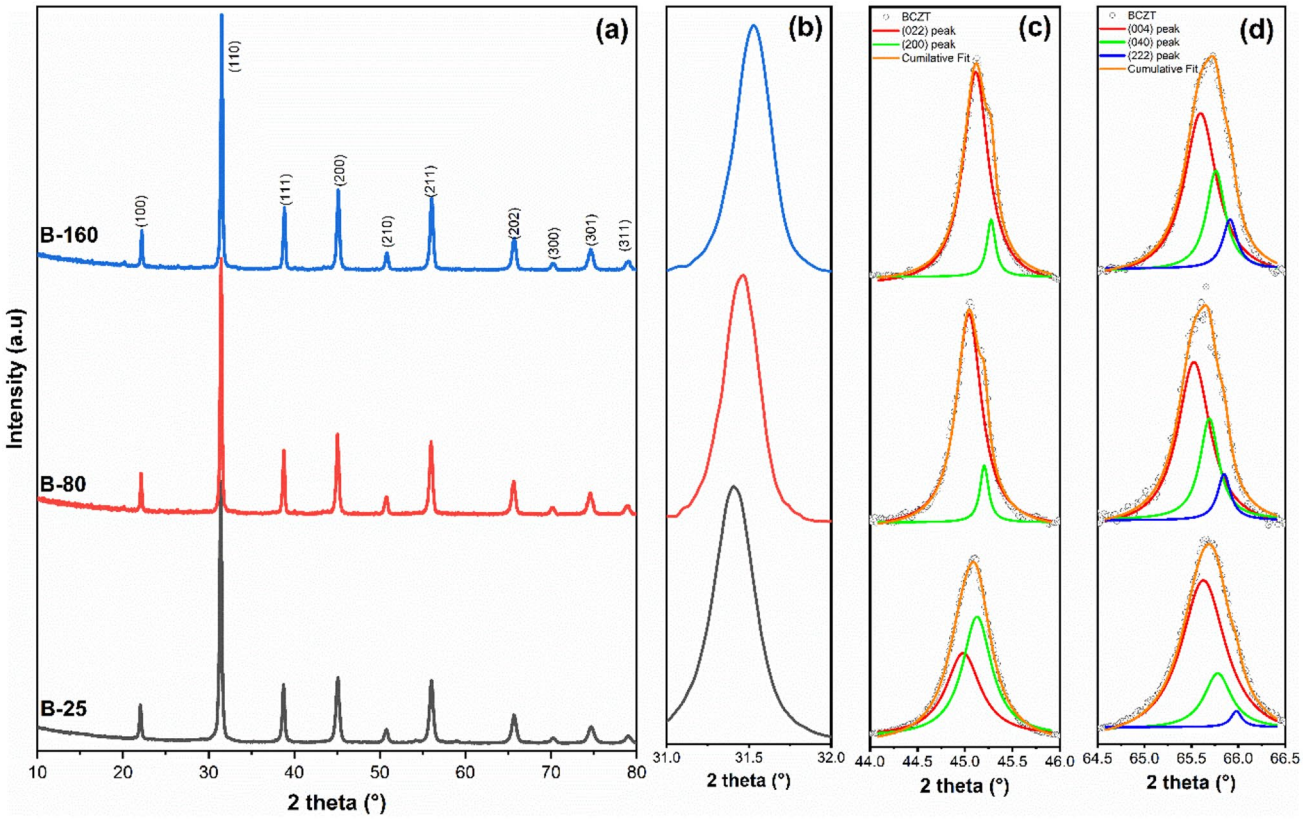

Fig. 2 **a** XRD patterns, **b** enlarged peak at $2\theta \approx 31.5°$ and peak splitting around **c** $2\theta \approx 45°$ and **d** $2\theta \approx 65.8°$ of B-25, B-80, and B-160 ceramics sintered at 1250 °C/10 h

Here, T_{dev} designates the temperature below which ε_r starts to deviate from the Curie–Weiss law, and T_m denotes the temperature at which ε_r value reaches the maximum. The calculated ΔT_m of B-25, B-80, and B-160 ceramics is shown in Table 1. The highest value was found to be 37 °C for B-80. However, the lowest ΔT_m was determined in B-25 ceramic.

For all ceramics, the Curie constant value is in the order of 10^5 K. This designates a typical well-known displacive-type ferroelectrics, *e.g.*, a high-temperature ferroelectric phase is driven by a displacive phase transition [25]. To evaluate this phase transition diffuseness, Eq. (3) is classically used [26].

$$\frac{1}{\varepsilon_r} - \frac{1}{\varepsilon_m} = \frac{(T - T_0)^{\gamma}}{C} (1 < \gamma < 2), \tag{3}$$

where ε_r, ε_m are the real part of the dielectric permittivity and its maximum value, respectively, and γ (degree of diffuse transitions) and C are constants. It is worth noting that γ is the exponent of the temperature dependence of the dielectric constant into the paraelectric phase, which would change from 1 (non-diffuse, Curie–Weiss law) to 2 (diffuse, Smolenskii–Isupov law). However, although largely used as a constant, this gamma parameter is in fact temperature dependent. It is only an average constant, depending on the temperature interval considered. In order to make a more correct comparison between the different samples, the same temperature interval was considered for all samples. Figure 4b, d, f shows the plot of $ln\ (1/\varepsilon_r - 1/\varepsilon_m)$ as a function of $ln\ (T - T_m)$ at 1 kHz for all BCZT ceramics. The linear fitting of these curves allows the obtention of γ values for BCZT ceramics. The obtained γ values are 1.34, 1.98, and 1.60 for B-25, B-80, and B-160 ceramics, respectively. B-80 and B-160 ceramics exhibit high γ values, hence, at a certain value of grain size, the increase in the grain size enhances the relaxor behavior, however, a further increase in the grain size, diminishes the relaxor behavior, this phenomenon was observed by Zheng et al. [27] and Bharathi et al. [25]. Furthermore, the grain size distribution (the presence of fine grains and coarse grains) could affect the relaxor behavior in BCZT ceramics [11]. Other plausible cause could be due to the compositional fluctuation and/or structural disordering in the arrangement of cation(s) in one or more crystallographic sites causing a microscopic heterogeneity in the compound [28–30].

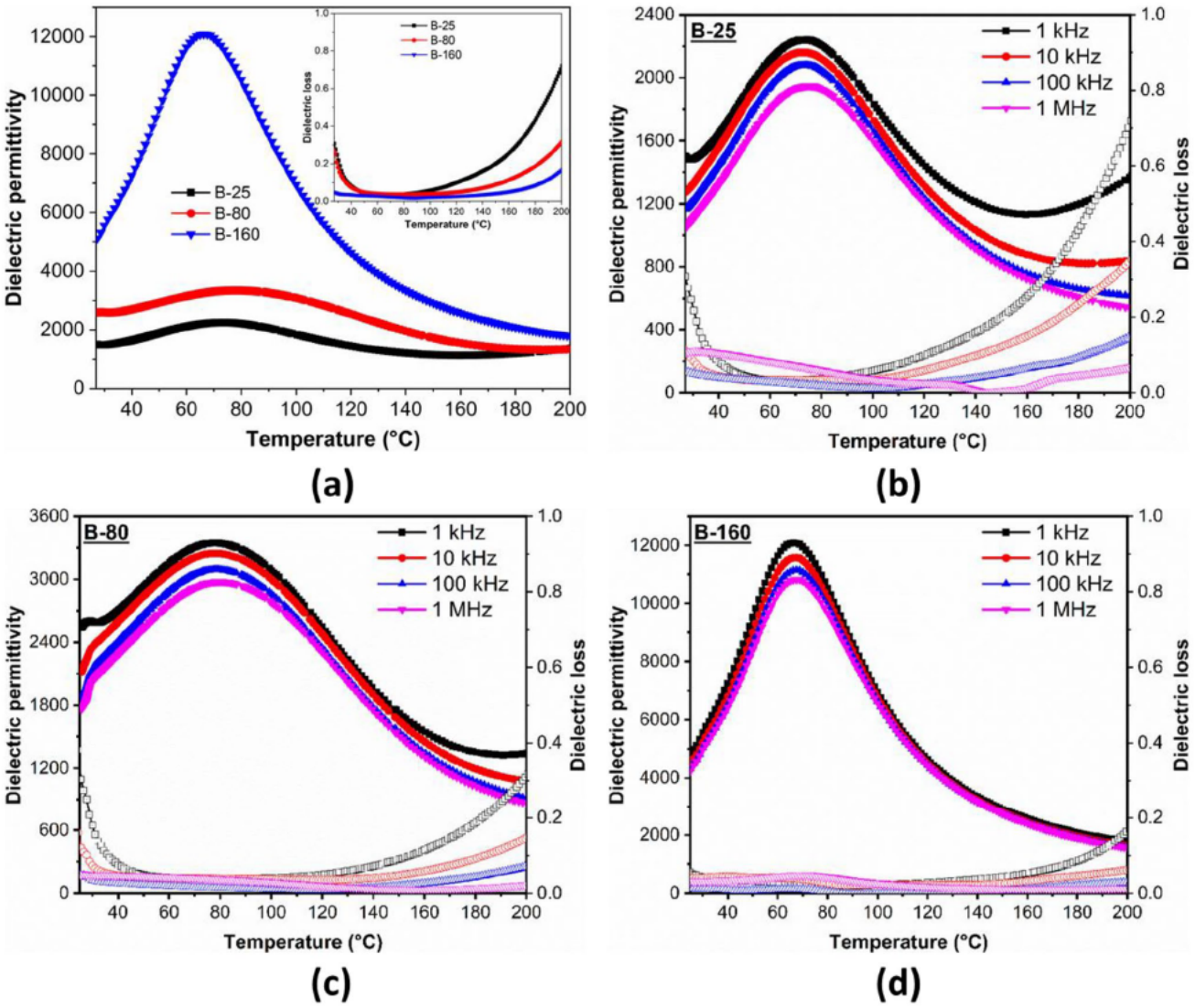

Fig. 3 **a** Comparison of the dielectric properties of BCZT ceramics at 1 kHz, and temperature dependence of the dielectric permittivity and dielectric loss of **b** B-25, **c** B-80, and **d** B-160 ceramics sintered at 1250 °C/10 h

Table 1 Relaxor properties at 1 kHz of B-25, B-80, and B-160 ceramics sintered at 1250 °C/10 h

	ε_m	$tan\ \delta$	Grain size (μm)	T_0 (°C)	$C\times 10^5$ (K)	T_m (°C)	T_{dev} (°C)	ΔT_m (°C)	γ
B-25	2242	0.035	0.8	21	0.72	74	87	13	1.34
B-80	3346	0.037	2.5	58	0.80	78	115	37	1.98
B-160	12,085	0.017	22.1	71	2.33	66	95	29	1.60

3.4 Ferroelectric properties

To have an insight on the ferroelectric properties of BCZT ceramics, room-temperature *P–E* loops under 20 kV/cm and 10 Hz were plotted in Fig. 5a. Interestingly, it was demonstrated for the first time that the ceramic elaborated at room temperature (B-25) exhibits a ferroelectric behavior evidenced by the *P–E* hysteresis loops. The remnant polarization (P_r) increases from 0.81 to 2.80 and 4.52 μC/cm^2 for B-25, B-80, and B-160, respectively. In contrast, the coercive field (E_c) decreases from 3.63 to 3.97 and 3.21 kV/cm for B-25, B-80, and B-160, respectively. It is well known that the ferroelectric properties are highly dependent on parameters like grain size, grain

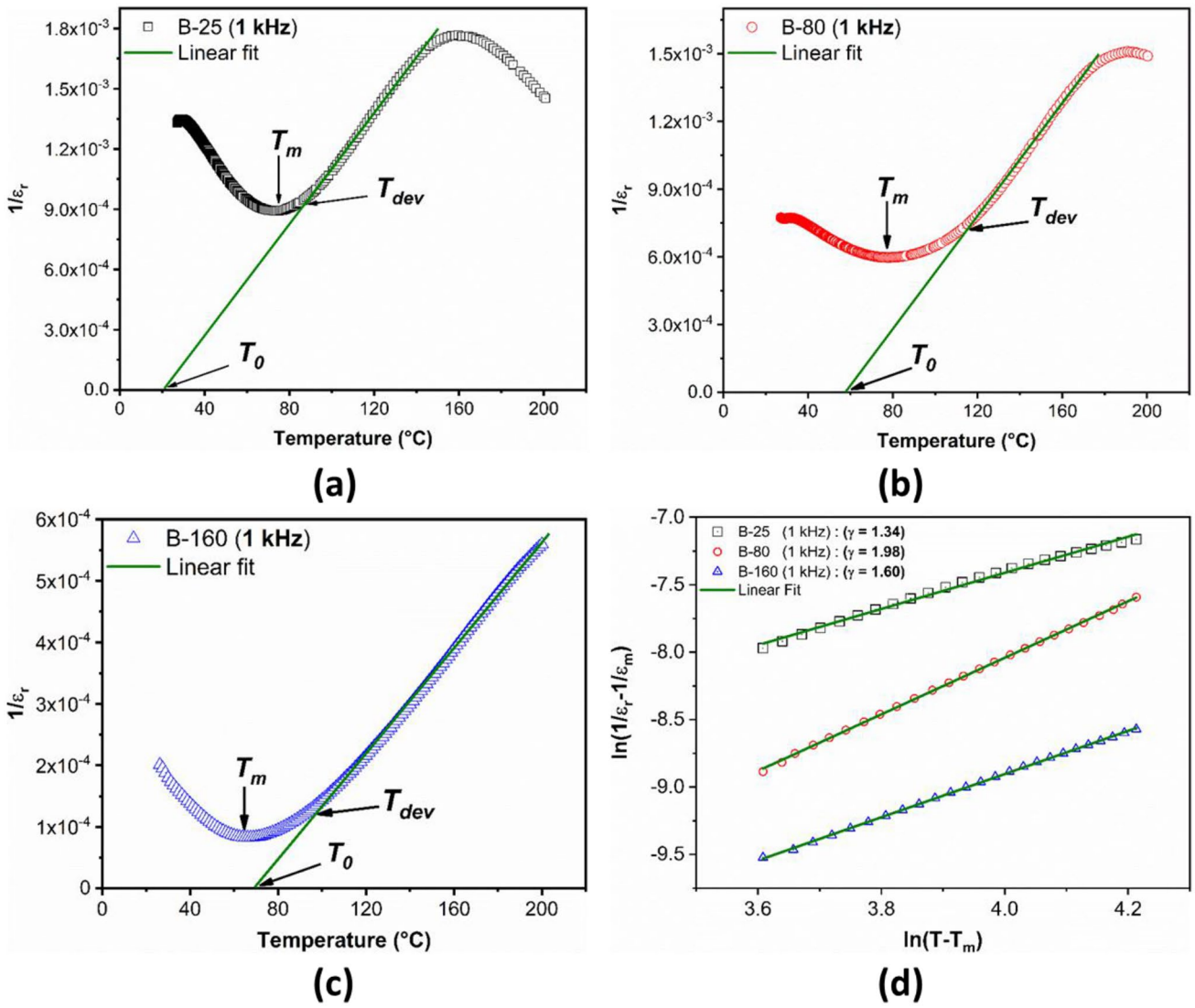

Fig. 4 Plots of Curie–Weiss relation for **a** B-25, **b** B-80, and **c** B-160 ceramics sintered at 1250 °C/10 h, and **d** modified Curie–Weiss law to determine slope (γ)

size distribution, grain shape, phase transition, ionic radii, and defect concentration [31–33]. The ceramics with large grains have been reported to exhibit larger P_r and small E_c [25, 34, 35]. Since the smaller grains in ferroelectric ceramics inhibit the formation of large ferroelectric domains, consequently, the effective contribution to the total polarization is reduced [27, 36]. Moreover, the grain boundary affects the polarization, since the grain boundary is a low-permittivity region, i.e., the grain boundary has poor ferroelectricity. Therefore, the polarization of the grain boundary may be low, or even zero. Space charges in the grain boundary exclude polarization charge on the grain surface, and a depletion layer on the grain surface can be formed. This results in the polarization discontinuity on the grain surface resulting in the depolarization field, and hence, polarization decreases [34]. The number of grain boundaries increases as the grain size decreases. Consequently, the remnant polarization decreases as the grain size decreases. Therefore, by increasing the synthesis temperature, the increase in grain size occurs resulting in enhancement of the ferroelectric properties.

Interestingly, the non-saturated *P–E* loop in B-160 ceramics could help to further increase in the applied electric field. Figure 5b depicts the hysteresis loops of B-160 ceramic at various electric fields from 10 to 60 kV/cm. It is shown that B-160 ceramic exhibits enhanced ferroelectric properties, the maximal polarization (P_{max}), and P_r increases with the increasing of the applied electric field. Under 60 kV/cm, P_{max} and P_r achieved 27.21 μC/cm^2, 8.59 μC/cm^2, respectively. The excellent ferroelectric properties

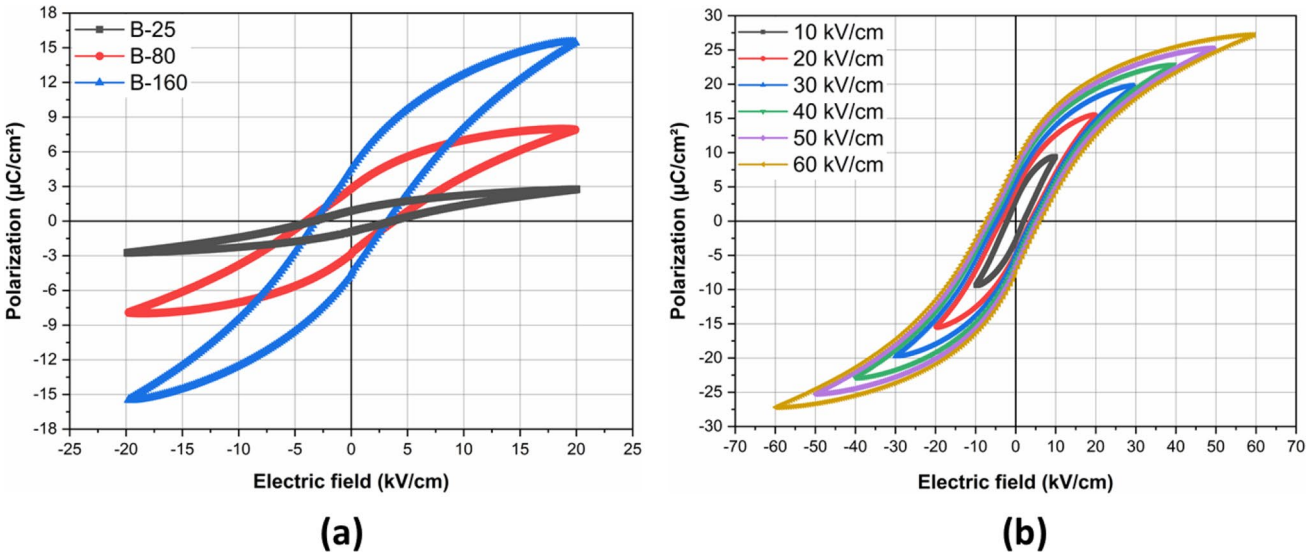

Fig. 5 **a** Room-temperature *P–E* loops of BCZT ceramics under 20 kV/m and **b** *P–E* loops of B-160 ceramic under various applied electric fields at 10 Hz

in B-160 ceramics further confirm the advantages of the low-temperature hydrothermal processing.

To illustrate the advantages of the low-temperature hydrothermal processing in lead-free BCZT ceramics elaboration, Table 2 summarizes the grain size average, relative density, and dielectric and ferroelectric properties of $Ba_{0.85}Ca_{0.15}Ti_{0.9}Zr_{0.1}O_3$ (BCZT) ceramics elaborated by different conditions of synthesis and methods. From energy consumption view, the synthesis temperature of BCZT powders with high dielectric and ferroelectric properties could be decreased to a low temperature of 160 °C, which is about 1000 − 1200 °C lower when compared with solid-state reaction and 640–840 °C lower when compared with sol–gel methods, respectively. Among the big advantage of "calcination-free" in hydrothermal and sol–gel hydrothermal processing, these strategies allow the synthesis of BCZT ceramics with enhanced dielectric and ferroelectric properties. For instance, B-160 ceramic processes a maximal dielectric constant of 12,085 higher than BCZT ceramics elaborated by solid-state and sol–gel hydrothermal processing, while keeping low dielectric loss. Moreover, from energy storage consideration, according to the following equations, large dielectric breakdown strength, a reduced remnant polarization, and large maximal polarization will lead to improved recoverable energy density and energy storage efficiency [37]. In other words, the charge storage density ($Q_c = P_{max} – P_r$) in a ferroelectric capacitor calculated from the ferroelectric hysteresis loops at zero field must be maximal to obtain high energy storage ferroelectric capacitor [38]. These requirements are gathered in BCZT ceramics elaborated by hydrothermal processing. B-160 could withstand high electric field (60 kV/cm) and shows $Q_c = 18.62$ μC/cm^2.

At 60 kV/cm, the obtained total energy density (W_{tot}) and recoverable energy density (W_{rec}) are 546.1 mJ/cm^3 and 367.2 mJ/cm^3, respectively, which corresponds to an energy efficiency $\eta = 67.2\%$. In BCZT ceramics with the same composition and at 60 kV/cm, Xu et al. [39] and Puli et al. [38] obtained W_{rec} of 121.6 mJ/cm^3 ($\eta = 51.3\%$) and 280 mJ/cm^3 ($\eta = 58.3\%$), respectively. These values are lower than those obtained in B-160 ceramics. Hence, the low-temperature hydrothermal route could be suitable for the design of energy-harvesting systems with improved performances.

$$W_{tot} = \int_0^{P_{max}} EdP, \tag{4}$$

$$W_{rec} = \int_{P_r}^{P_{max}} EdP, \tag{5}$$

$$\eta(\%) = \frac{W_{rec}}{W_{tot}} \times 100, \tag{6}$$

where W_{tot}, W_{rec}, and η are total energy density, recoverable energy density, and energy efficiency, while P_{max}, P_r, E, and P represent maximal polarization, remnant polarization, electric field, and polarization, respectively.

Table 2 Comparison of the dielectric and ferroelectric properties of lead-free BCZT ceramics reported here with others reported in literature using different synthesis conditions and methods

Synthesis conditions			Grain size (μm)	Relative density (%)	ε_m	tan δ	P_r (μC/cm^2)	P_{max} (μC/cm^2)	Q_c (μC/cm^2)	E kV/cm	Refs
Method	Calcination	Sintering									
Hydrothermal	No	1250 °C/10 h	22.1	97.1	12,085	0.017	8.59	27.21	18.62	60	This work
Sol–gel–hydrothermal	No	1400 °C/2 h	–	95	9173	–	12.56	41.00	28.44	40	[17]
Hydrothermal	No	1300 °C/3 h	12.09	–	7760	0.1	10.83	25.00	14.17	15	[12]
Solvothermal	1000 °C/4 h	1250 °C/10 h	6.6	96.4	9646	0.012	3.92	7.56	3.64	6.6	[22]
Sol–gel	1000 °C/4 h	1420 °C/6 h	–	–	16,480	0.015	11.60	17.76	6.16	30	[7]
Sol–gel	800 °C	1400 °C/2 h	–	95	8808	0.02	12.20	17.23	5.03	30	[40]
Sol–gel	1000 °C/4 h	1550 °C/2 h	10	97	20,250	–	10.70	20.70	10.00	50	[41]
Sol–gel auto-combustion	1200 °C/2 h	1450 °C/2 h	3.4	97	–	–	7.38	15.50	8.12	20	[13]
Solid-state	1150 °C/6 h	1400 °C/6 h	–	95	10,615	–	8.21	18.53	10.32	50	[42]
Solid-state	1147 °C/12 h	1427 °C/2 h	–	–	4762	0.022	4.35	6.53	2.18	8	[43]
Solid-state	1350 °C and 1400 °C/6 h	1450 °C/4 h	–	94	–	–	5.48	16.06	10.58	21	[44]

4 Conclusions

Structural, morphological, dielectric, and ferroelectric properties of three lead-free BCZT ceramics (B-25, B-80, and B-160) prepared via hydrothermal route at very-low temperature (≤ 160 °C) have been investigated. X-ray diffraction demonstrated that all BCZT samples were crystallized in a pure perovskite phase with the coexistence of orthorhombic/tetragonal structure at room temperature. Increasing the hydrothermal treatment, i.e., increasing grain size, enhanced the dielectric and ferroelectric properties of BCZT ceramics. In B-160 ceramic, the ceramic density reached 97.1%, and the dielectric constant and dielectric loss values at the maximum of the temperature peak of the dielectric constant were 12,085 and 0.017, respectively. Moreover, high values of the recovered energy density of 367.2 mJ/cm^3 and the energy efficiency of 67.2% were obtained in B-160. Therefore, the hydrothermal method has better advantages on the elaboration of BCZT ceramics at lower sintering temperature and with enhanced electrical properties and high energy performances.

Acknowledgements The authors gratefully acknowledge the generous financial support of CNRST Priority Program PPR 15/2015 and the European Union's Horizon 2020 research and innovation program under the Marie Skłodowska-Curie grant agreement No. 778072. Z. K. and B. R. acknowledge Slovenian Research Agency grant J1-9147 and program P1-0125.

References

1. Z. Zhou, H. Tang, H.A. Sodano, Adv. Mater. **26**, 7547 (2014)
2. J. Koruza, A.J. Bell, T. Frömling, K.G. Webber, K. Wang, J. Rödel, J. Mater. **4**, 13 (2018)
3. J. Gao, D. Xue, W. Liu, C. Zhou, X. Ren, Actuators **6**, 24 (2017)
4. P.K. Panda, B. Sahoo, Ferroelectrics **474**, 128 (2015)
5. J. Rödel, W. Jo, K.T.P. Seifert, E.M. Anton, T. Granzow, D. Damjanovic, J. Am. Ceram. Soc. **92**, 1153 (2009)
6. W. Liu, X. Ren, Phys. Rev. Lett. **103**, 257602 (2009)
7. Z. Wang, J. Wang, X. Chao, L. Wei, B. Yang, D. Wang, Z. Yang, J. Mater. Sci. Mater. Electron. **27**, 5047 (2016)
8. J.P. Praveen, T. Karthik, A.R. James, E. Chandrakala, S. Asthana, D. Das, J. Eur. Ceram. Soc. **35**, 1785 (2015)
9. M.A. Rafiq, M.N. Rafiq, K. Venkata Saravanan, Ceram. Int. **41**, 11436 (2015)
10. J. Shi, R. Zhu, X. Liu, B. Fang, N. Yuan, J. Ding, H. Luo, Materials (Basel). **10**, 1093 (2017)
11. Z. Hanani, D. Mezzane, M. Amjoud, S. Fourcade, A.G. Razumnaya, I.A. Luk'yanchuk, M. Gouné, Superlattices Microstruct. **127**, 109 (2019)
12. S. Hunpratub, S. Maensiri, P. Chindaprasirt, Ceram. Int. **40**, 13025 (2014)
13. P. Jaimeewong, M. Promsawat, A. Watcharapasorn, S. Jiansirisomboon, Integr. Ferroelectr. **175**, 25 (2016)
14. Z. Hanani, E.H. Ablouh, M.B. Amjoud, D. Mezzane, S. Fourcade, M. Gouné, Ceram. Int. **44**, 10997 (2018)

15. C. Baek, J. E. Wang, S. Ryu, J. H. Kim, C. K. Jeong, K. Il Park, and D. K. Kim, RSC Adv. **7**, 2851 (2017).
16. T. Maiti, R. Guo, A.S. Bhalla, J. Appl. Phys. **100**, 114109 (2006)
17. X. Ji, C. Wang, S. Zhang, R. Tu, Q. Shen, J. Shi, L. Zhang, J. Mater. Sci. Mater. Electron. **30**, 12197 (2019)
18. C. Chen, Y. Wei, X. Jiao, D. Chen, Mater. Chem. Phys. **110**, 186 (2008)
19. Z. Chen, Z. Li, J. Qiu, T. Zhao, J. Ding, X. Jia, W. Zhu, J. Xu, J. Eur. Ceram. Soc. **38**, 1349 (2018)
20. G.K. Sahoo, R. Mazumder, J. Mater. Sci. Electron. **25**, 3515 (2014)
21. D.S. Keeble, F. Benabdallah, P.A. Thomas, M. Maglione, J. Kreisel, Appl. Phys. Lett. **102**, 092903 (2013)
22. Z. Hanani, D. Mezzane, M. Amjoud, A.G. Razumnaya, S. Fourcade, Y. Gagou, K. Hoummada, M. El Marssi, M. Gouné, J. Mater. Sci. Mater. Electron. **30**, 6430 (2019)
23. A. A. Bokov, Z.-G. Ye, in *Front. Ferroelectr. SE—4* (Springer US, Boston, MA, 2007), pp. 31–52.
24. Y. Liu, Y. Pu, Z. Sun, Mater. Lett. **137**, 128 (2014)
25. P. Bharathi, K.B.R. Varma, J. Appl. Phys. **116**, 164107 (2014)
26. K. Uchino, S. Nomura, Ferroelectr. Lett. Sect. **44**, 55 (1982)
27. C. Zhang, F. Chen, X. Zhong, Z. Ling, Z. Tang, G. Jian, J. Mater. Sci. Mater. Electron. **29**, 16730 (2018)
28. D. Hennings, A. Scnell, G. Simon, J. Am. Ceram. Soc. **65**, 539 (1982)
29. Y. Tian, X. Chao, L. Wei, P. Liang, Z. Yang, J. Appl. Phys. **113**, 184107 (2013)
30. I. Coondoo, N. Panwar, D. Alikin, I. Bdikin, S.S. Islam, A. Turygin, V.Y. Shur, A.L. Kholkin, Acta Mater. **155**, 331 (2018)
31. C.G.F. Stenger, A.J. Burggraaf, J. Phys. Chem. Solids **41**, 17 (1980)
32. K.M. Sangwan, N. Ahlawat, R.S. Kundu, S. Rani, S. Rani, N. Ahlawat, S. Murugavel, J. Phys. Chem. Solids **117**, 158 (2018)
33. Z. Hanani, S. Merselmiz, A. Danine, N. Stein, D. Mezzane, M. Amjoud, M. Lahcini, Y. Gagou, M. Spreitzer, D. Vengust, Z. Kutnjak, M. El Marssi, I.A. Luk 'yanchuk, M. Gouné, J. Adv. Ceram. **9**, 210 (2020)
34. W. Cai, Y. Fan, J. Gao, C. Fu, X. Deng, J. Mater. Sci. Mater. Electron. **22**, 265 (2011)
35. Y. Tan, J. Zhang, Y. Wu, C. Wang, V. Koval, B. Shi, H. Ye, R. McKinnon, G. Viola, H. Yan, Sci. Rep. **5**, 9953 (2015)
36. J. Zhai, X. Yao, J. Shen, L. Zhang, H. Chen, J. Phys. D **37**, 748 (2004)
37. Y. Huang, F. Li, H. Hao, F. Xia, H. Liu, S. Zhang, J. Mater. **5**, 385 (2019)
38. V.S. Puli, D.K. Pradhan, I. Coondoo, N. Panwar, S. Adireddy, S. Luo, R.S. Katiyar, D.B. Chrisey, J. Phys. D **52**, 255304 (2019)
39. K. Xu, P. Yang, W. Peng, L. Li, J. Alloys Compd. **829**, 154516 (2020)
40. X. Ji, C. Wang, S. Li, S. Zhang, R. Tu, Q. Shen, J. Shi, L. Zhang, J. Mater. Sci. Mater. Electron. **29**, 7592 (2018)
41. E. Chandrakala, J. Paul Praveen, B.K. Hazra, D. Das, Ceram. Int. **42**, 4964 (2016)
42. X. Wang, P. Liang, X. Chao, Z. Yang, J. Am. Ceram. Soc. **98**, 1506 (2015)
43. H. Kaddoussi, A. Lahmar, Y. Gagou, B. Manoun, J.N. Chotard, J.L. Dellis, Z. Kutnjak, H. Khemakhem, B. Elouadi, M. El Marssi, J. Alloys Compd. **713**, 164 (2017)
44. S. Patel, D. Sharma, A. Singh, R. Vaish, J. Mater. **2**, 75 (2016)